



Exploration of Geothermal Resources Utilizing Geophysical and Borehole Data in the Abu Gharadig Basin of Egypt's Northern Western Desert

AHMED ELMASRY,^{1,3} MOHAMED ABDEL ZAHER,² AHMED MADANI,³ and TAMER NASSAR³

Abstract—The Abu Gharadig Basin is regarded as one of the most essential in Egypt, serving as the country's second most important reservoir for hydrocarbon production. Our present study is focused on the investigation of geothermal resources in the Abu Gharadig Basin. Using airborne magnetic and gravity surveys, as well as temperature well records, we can identify possible geothermal sources in this region. Power spectral analysis was used on the airborne magnetic measurements to compute the Curie Point Depths (CPDs) and display the temperature gradients and heat flows regime in the study area, while on the gravity data, 3-D density inversion was used to identify the basement surface. Real data from bottom-hole temperature (BHT) logs and geological data (structural and stratigraphic data from prior studies) were used to cross-validate the geophysical maps and to ascertain the stratigraphy and structural setting beneath the study location. The depth of the basement rock, according to the studies, ranges from 4.5 to 7 km, and the CPDs run from 17 to 22 km. Furthermore, the estimated temperature gradients vary from 25 to 34 degrees Celsius per kilometer, whereas the heat flows vary from 52 to 86 mW/m². Generally, there is a correlation between shallow curie depths, uplifts on basement rocks, and sites of high heat flow, indicating that basement rocks are primarily accountable for the geothermal potential of the basin.

Keywords: Renewable energy, geothermal resources, aerogravity, aeromagnetic, bottom-hole temperature.

1. Introduction

Two-thirds of Egypt's overall region is covered by the Western Desert and has a special importance because it contained different petroliferous basins that contain high potential of hydrocarbon, which it

considered the second area in Egypt to produce the hydrocarbon (Meshref et al., 1988). It is distinguished by a complicated subsurface structure framework (Salem, 1976) and the presence of groundwater of the Nubian sandstone aquifer and thick sedimentary cover. The Abu Gharadig Basin (AGB) is considered to be the most promising areas of hydrocarbon potentialities and important sedimentary basin in the Western Desert (Awad, 1984; Bayoumi & Lotfy, 1989). It comprises around 3.6% of the Western Desert and is regarded as one of Egypt's key basins. It is an intracratonic, circular half-graben with an asymmetric E-W trend. AGB has around 330 km in length and 50 to 75 km in width. It is bordered by the Qattara Ridge to the north and the Sitra Platform to the south (Abdel Aal & Moustafa, 1988) (Fig. 1).

Many studies have been conducted to investigate the groundwater and geothermal potentials in various locations of Egypt, but relatively few have concentrated on the AGB (e.g., Abdel Zaher et al., 2012, 2014; Atef et al., 2016; Boulos, 1990; Elbarbary et al., 2021; Madani & Said, 2022; Mohamed & Abdel Zaher, 2020; Mohamed et al., 2016; Rabeh et al., 2018; Senosy et al., 2013). The majority of studies in the Western Desert especially the AGB is to investigate the structure and stratigraphy, but there are few researches to investigate the geothermal potentiality. Shazly (2012) used data from the available well logging to determine the suitable reservoir rock as well as assess the geothermal potential of the Lower and Upper Bahariya formation. Saada (2016) utilized airborne magnetic measurements to investigate the Curie point depth (CPD) and heat flux at the Northern section of the Western Desert in order to determine whether this area could be useful for petroleum exploration or geothermal energy in the

¹ Concord for Engineering and Contracting Company, New Maadi, Maadi, Cairo, Egypt.

² National Research Institute of Astronomy and Geophysics (NRIAG), Helwan, Cairo 11421, Egypt.

³ Geology Department, Faculty of Science, Cairo University, Cairo, Egypt. E-mail: nassart@cu.edu.eg

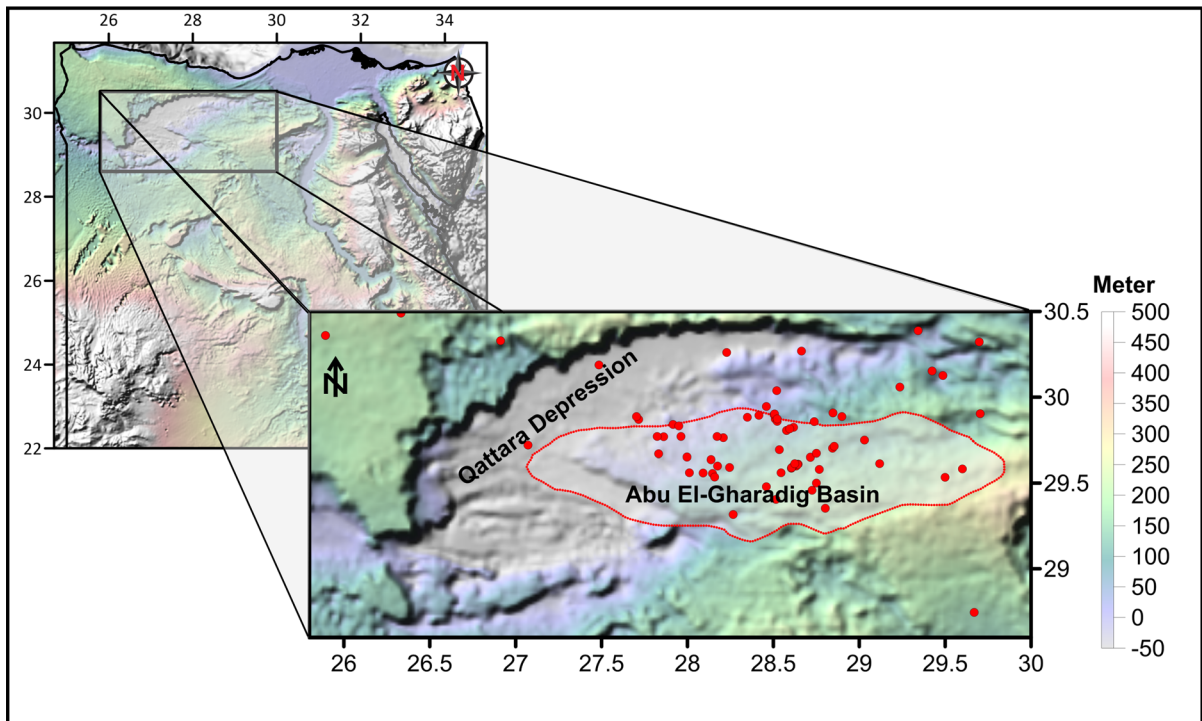


Figure 1

Location and topography (DEM from a satellite dataset) map of AGB in Egypt's Northern Western Desert. The outline of the Basin is shown by a red polygon, and the locations of the BHT wells are indicated by red dots

future. Using spectrum analysis of aeromagnetic data, Abdel Zaher et al. (2018a) estimated the CPD, geothermal gradient, and heat flow maps of the Siwa oasis. They also utilized 3D inversion on aerogravity data to identify the depths of basement rocks in the Siwa oasis. Depending on the power spectrum studies of aeromagnetic data, Elbarbary et al. (2018) developed the temperature gradients and heat fluxes maps for Egypt. Abdel Zaher et al. (2018b) integrated different datasets such as geophysical, aeromagnetic, aerogravity and geochemical data to assess the Farafra Oasis' geothermal potential in Western Desert. Lashin (2015) analyzed the most promising areas of geothermal potential and the geothermal activity in Egypt to give recommendations about the best areas to build and construct a geothermal power plant to generate energy. Madani (2020) used Thermal Infrared Remote Sensing and SAR techniques to detect geothermal anomalies in the Rift-Related Wadi

Natash Volcanic Field, South Eastern Desert, Egypt. Madani and Said (2022) identified the geothermal anomalies covered the Egyptian territories using Sentinel-3 Land Surface Temperature (LST) products.

The purpose of current research is to examine the subsurface structure of AGB and its relevance to the presence of geothermal energy resources using airborne potential field data. The CPD was computed using power spectrum analysis on aeromagnetic data, whereas the depths to the basement surface were determined using 3D inversion of gravity data. In addition, temperature records from 138 deep wells were utilized to map the temperature gradients and heat fluxes of AGB and to validate the results from geophysical data. This study assists in evaluating the geothermal potential of AGB for geothermal development and achieving optimal usage of geothermal resources in the northern Western Desert.

2. Geological and Structure Setting

The western desert mainly composed of a flat plateau, several depressions and oases (Sestini, 1995). The NW desert is divided into two regions by the Ras Qattara at N Sinai uplift (Meshref et al., 1988). The AGB is shaped like an oval with E-W orientation and is located in the central region of the NW Desert (Fig. 1). The AGB is bounded by the Qattara Ridge to the north and the Sitra Platform to the south. It is also flanked by Kattanya High to the east and Gib Afia High to the west (Demerdash et al., 1984). The sedimentary successions in the AGB range from 8 to 9 km, having ages from Precambrian to recent deposits (Hantar, 1990). There are unconformities between the sedimentary column and the basement rocks (El Ayouty, 1990). The AGB includes a high amount of half-graben structures and major graben structures (Wood, 1984).

The AGB is located in the unstable shelf zone, which has a thick sedimentary sequence underlain by basement rocks, and it is distinguished by a variety of tectonic features as a result of intense compressional and tensional movements (Said, 1962; Schlumberger, 1984). As a result of the North African plate moving closer to the Europe plate most of the important geologic events happened through the Late Cretaceous and Early Tertiary, the main portions of the NW Desert were uplifted and folded in almost NE to SW orientation (Syrian Arc system) (Said, 1962).

The AGB has a large-scale structural province in the NW Desert (Dolson et al., 1999; EGPC, 1992). From east to west, the Abu Gharadig anticline, the Mubarak High and the Mid Basin Arch are the dominant structural features in AGB, that divide the basin into several structural units (Fig. 2) (Meshref, 1990). The most common faults in the AGB are normal faults, and their main trends are EW, ENE, and WNW directions. Reverse faults are uncommon, and their trends are ENE and EW directions. Strike-slip faults are rarely detected (Sultan & Halim, 1988). Faults with significant displacements are limited to the NE to SW trend of the Kattaniya Horst and the EW trend of the Abu Gharadig garben; these large displacements occurred in the Post Turonian period

and had a higher impact on the distribution of sediments in the Late Cretaceous and Early Tertiary. Also, there are other structures in AGB belong to Late Cretaceous such as flower structures and revers fault (Bayoumi & Lotfy, 1989). We might state that there is a complicated situation with various structures in and around AGB that can accommodate several geothermal resources. On the other hand, geothermal fields are dependent on faults and structures because fluids often move via fissures in the underground rocks. This highlights the significance of faults and structures in the study of geothermal resources.

3. Data Used

The current study utilized temperature well records and the geophysical data (airborne gravity and magnetic) for geothermal investigation through AGB. Airborne gravity data in the form of a Bouguer anomaly map with a contour interval of 5 mGal (Fig. 3a) is considered to be one of the most important sources of information on the interior composition of the Earth's crust. The Getech group lc. provided the gravity information as a 10 km (5-min) grid of Bouguer anomaly and measured at 600 m above ground. On the other hand, GETECH also provided the airborne magnetic measurements in the shape of a consolidated 1000 m grid of total magnetic intensity (TMI) that was created using ground and aeromagnetic data, as well as Magsat data, at a mean terrain clearance of 1000 m, with 10 nT contour intervals and 3000 m line spacing (Green et al., 1992) (Fig. 3b).

The current study also include temperature well records from 138 wells that ranging in depth from 2000 to 4800 m (Fig. 1). These wells drilled by Egyptian General Company (EGPC), British Petroleum Company (BPC) and the Gulf of Suez Petroleum Company (GUPCO). Bottom hole temperatures (BHT), which are measured at the bottom of the well, are used to represent temperature information.

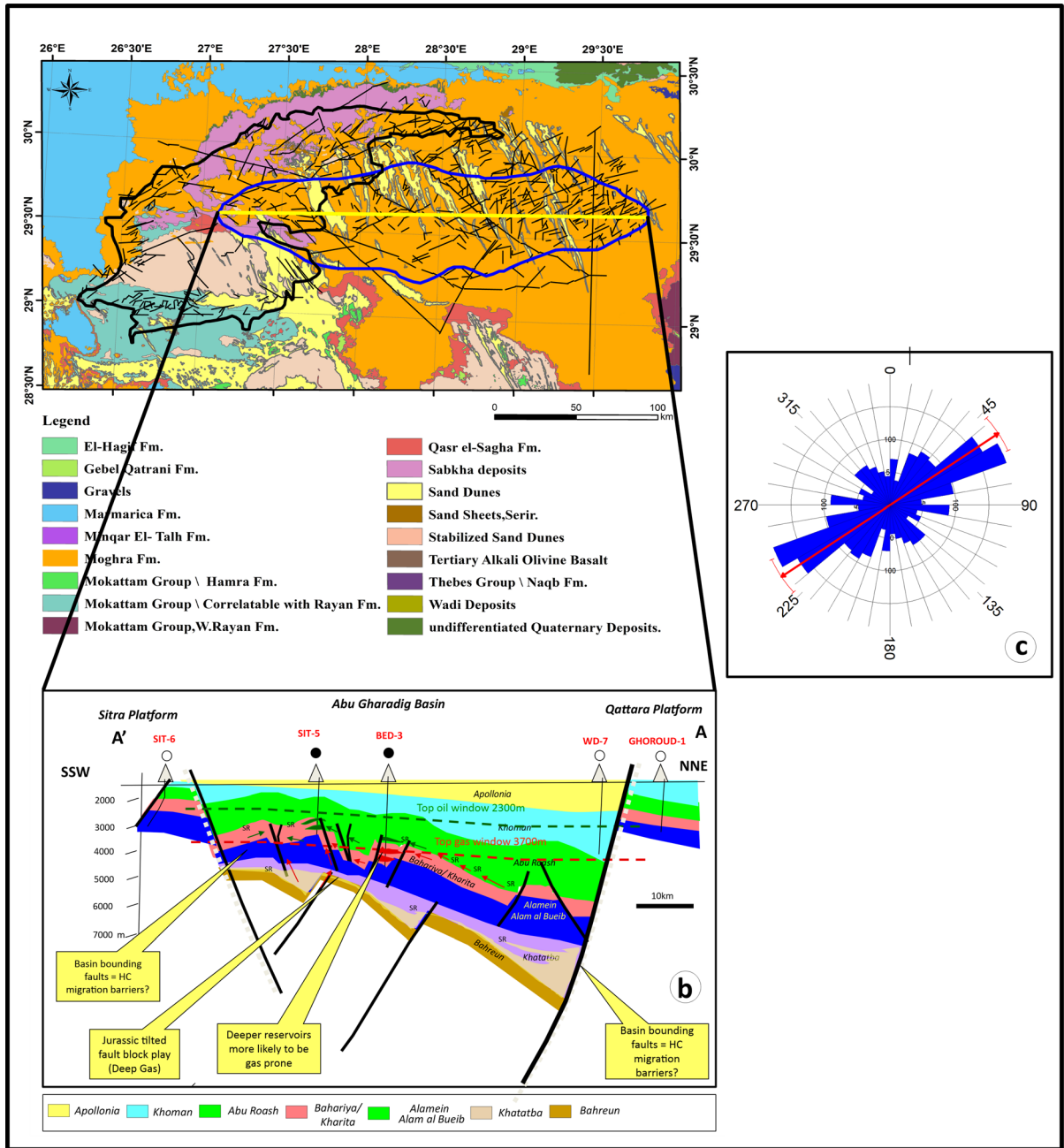


Figure 2

a Geological map of the northwestern desert (modifies after GSE, 1981); the structural lines are denoted by the black lines, **b** stratigraphic cross section through AGB, as described by Taha, 1992, Ayyad & Darwish, 1996 and **c** a rose diagram depicts the lineaments trends on the geological map

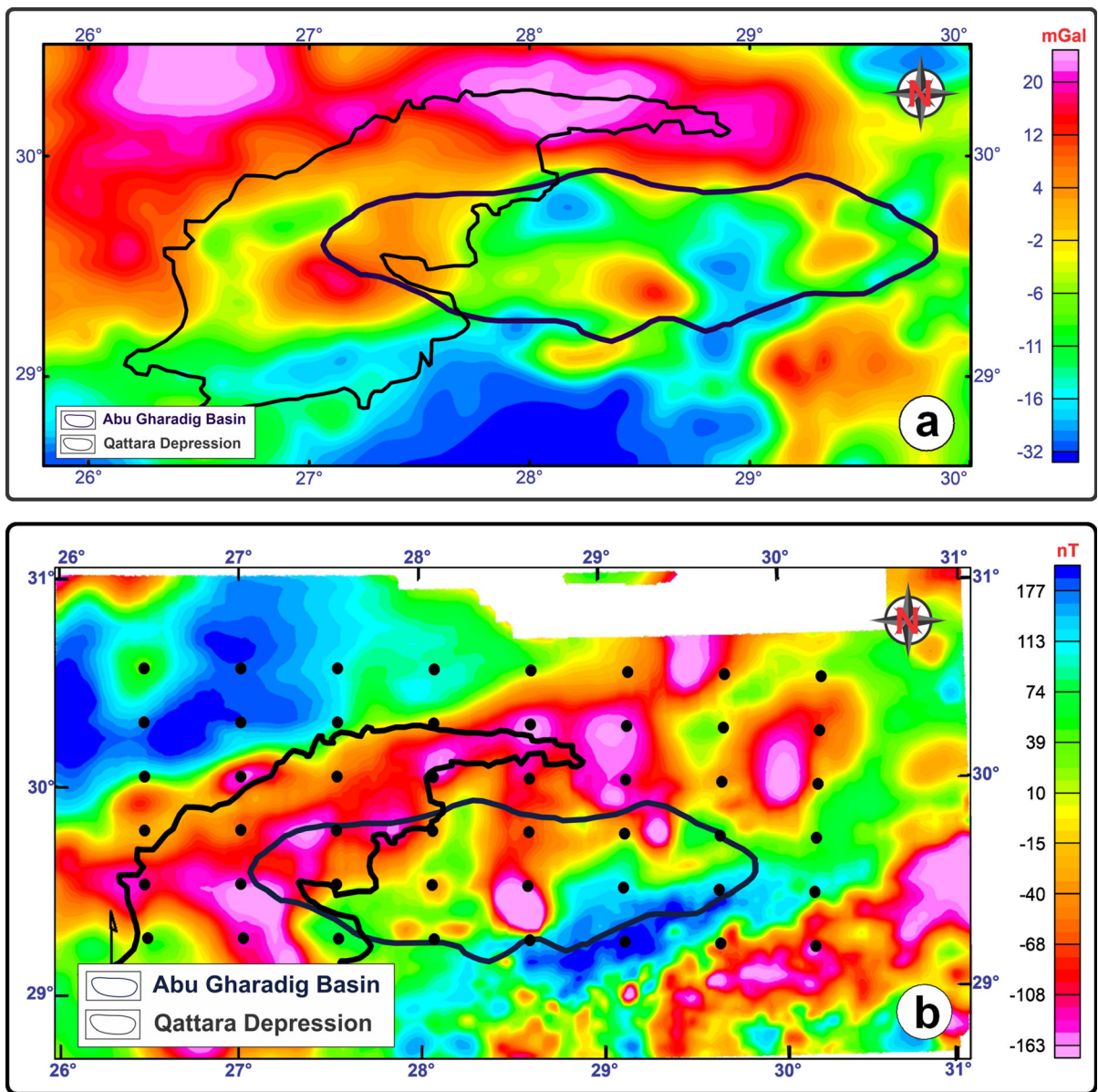


Figure 3

The study region's airborne geophysical maps include **a** Bouguer anomaly map and **b** RTP aeromagnetic map. The outlines of the AGB and Qattara Depression are represented by black polygons. On the RTP map, black dots indicate the positions of the centers of sub-areas utilized to compute the CPD depths

4. Methodology

4.1. Temperature Data

The temperature data is in the form of bottom hole temperatures (BHT), which are recorded at the well's bottom (i.e., the maximum temperature).

Temperature logs are taken on a regular basis, whether during drilling or shortly after circulation has stopped. The temperature readings are often smaller than the corresponding temperature of the formation because the drilling liquid infiltrates it and use heat convection to cool it. Therefore, corrections

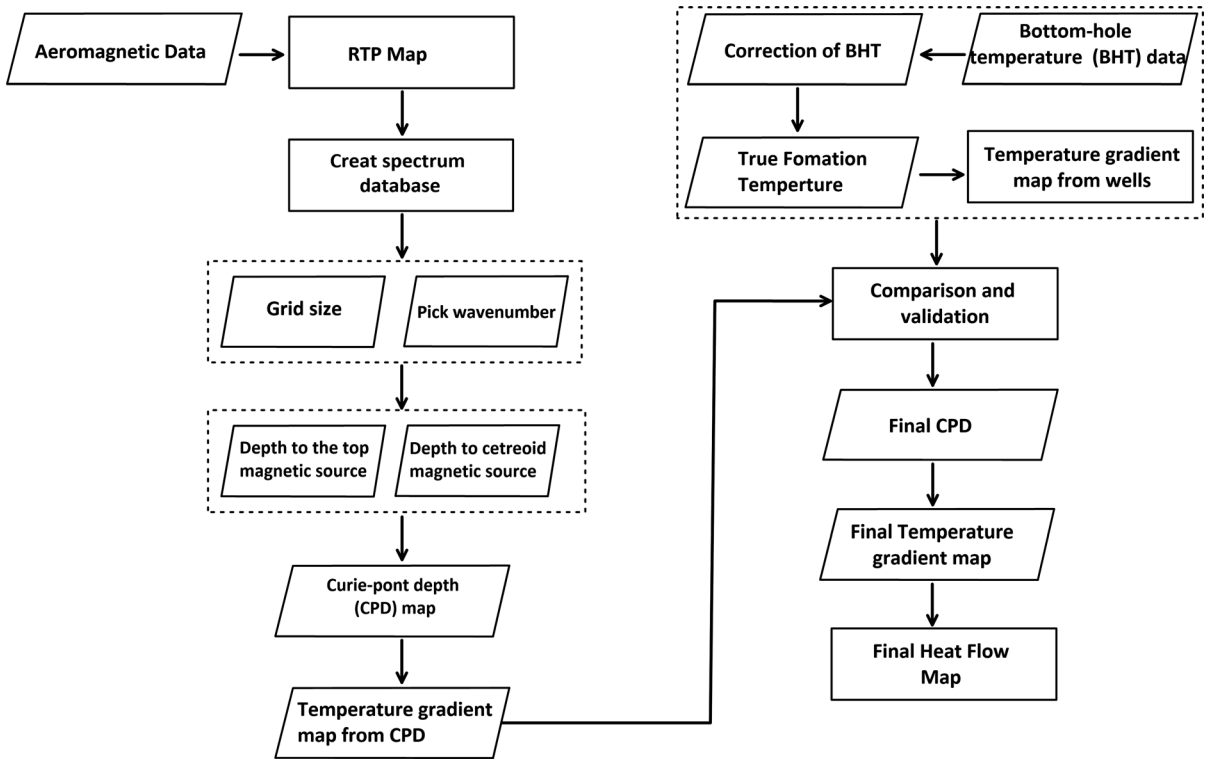


Figure 4

Methodology flowchart for calculating CPD, temperature gradients, and heat flow maps employing spectral analyses of aeromagnetic data

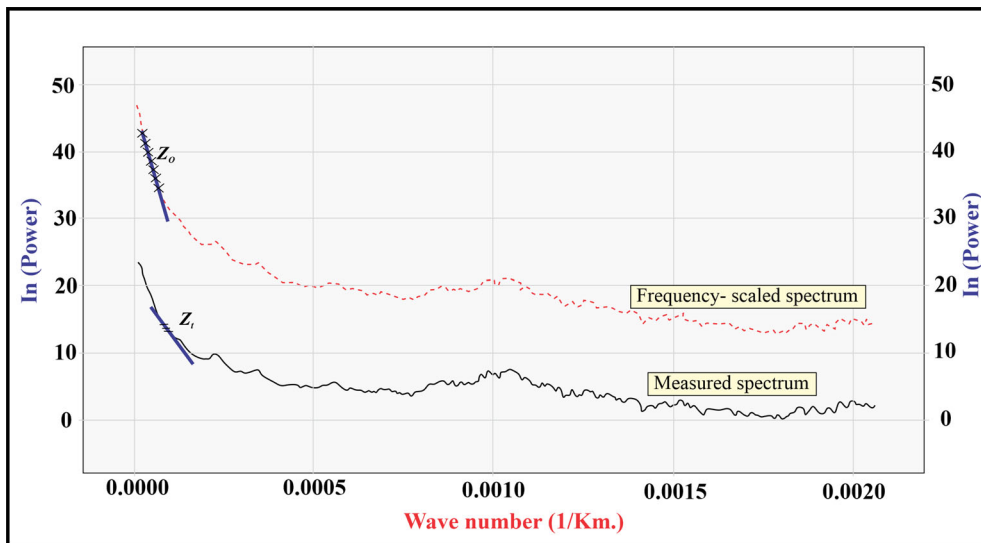


Figure 5

Example of the radial power spectrum of aeromagnetic data from window no. 48. The inclination of the greatest wavelength component of the spectrum was used to calculate the CPD

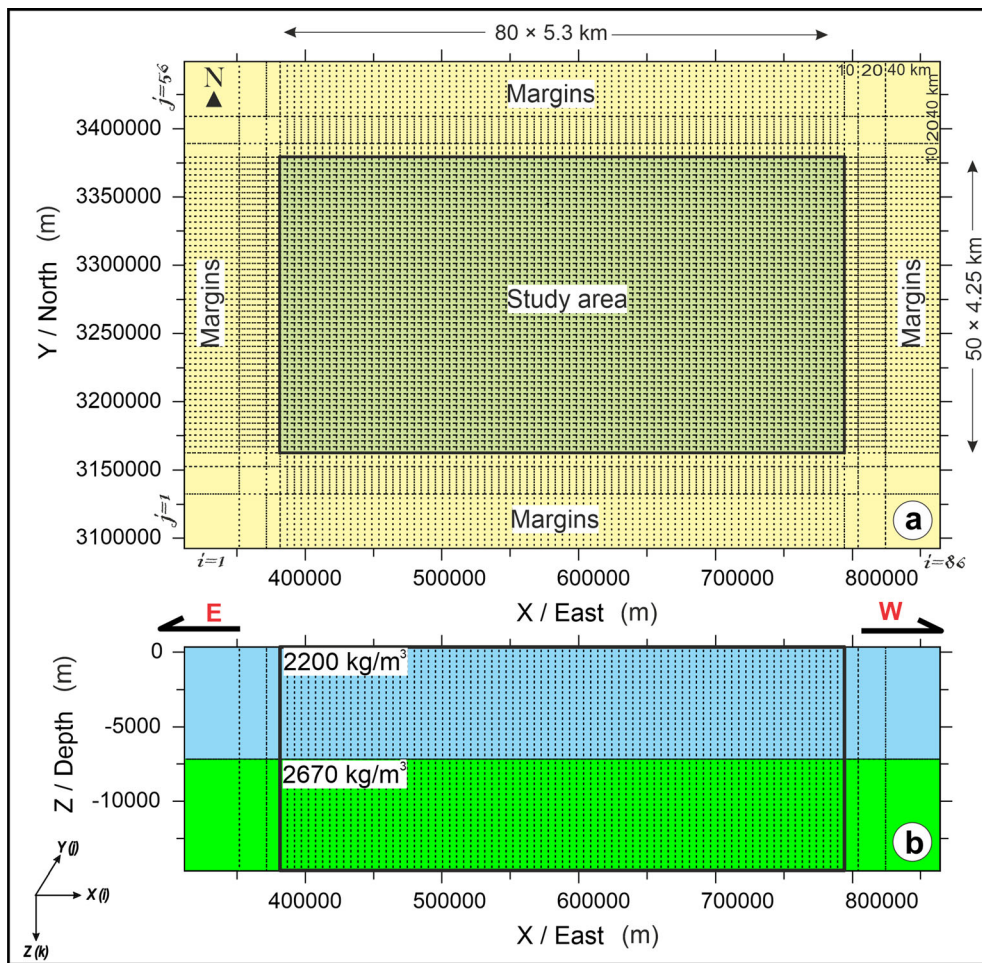


Figure 6

a Plane perspective of the grid blocks for the 3-D density model. **b** The E-W section for the two-layer scenario, consisting of the sedimentary layer and the basement layer. Projected coordinates (UTM zone 35N) are given in meters

are needed before determining the actual formation temperatures using the BHT data.

An empirical formula developed by Waples et al. (2004) was applied to our data in order to make the corrections. The formula is:

$$T_{\text{true}} = T_{\text{surf}} + (f \times (T_{\text{meas}} - T_{\text{surf}})) - (0.0014 \times (Z - 4498)) \quad (1)$$

In which T_{surf} refers to the sea floor temperature, T_{meas} refers to the temperature of a log in degrees Celsius (BHT), Z refers to the number of meters beneath the seabed, while the f refers to the correction factor and it indicates how much time has passed since the fluid has been stopped (T_{sc}):

$$f = [-0.146 \times \ln(T_{\text{sc}}) + 1.69] / (0.57 \times Z^{0.075}). \quad (2)$$

These equations, which were modified from those of Waples and Ramly (2001), were evaluated by Waples et al. (2004) using data from other geological provinces, demonstrating that they can be utilized with a high degree of confidence in many or the vast majority of other geological regions.

Then, we may use the corrected BHT for estimating the temperature gradient using this equation:

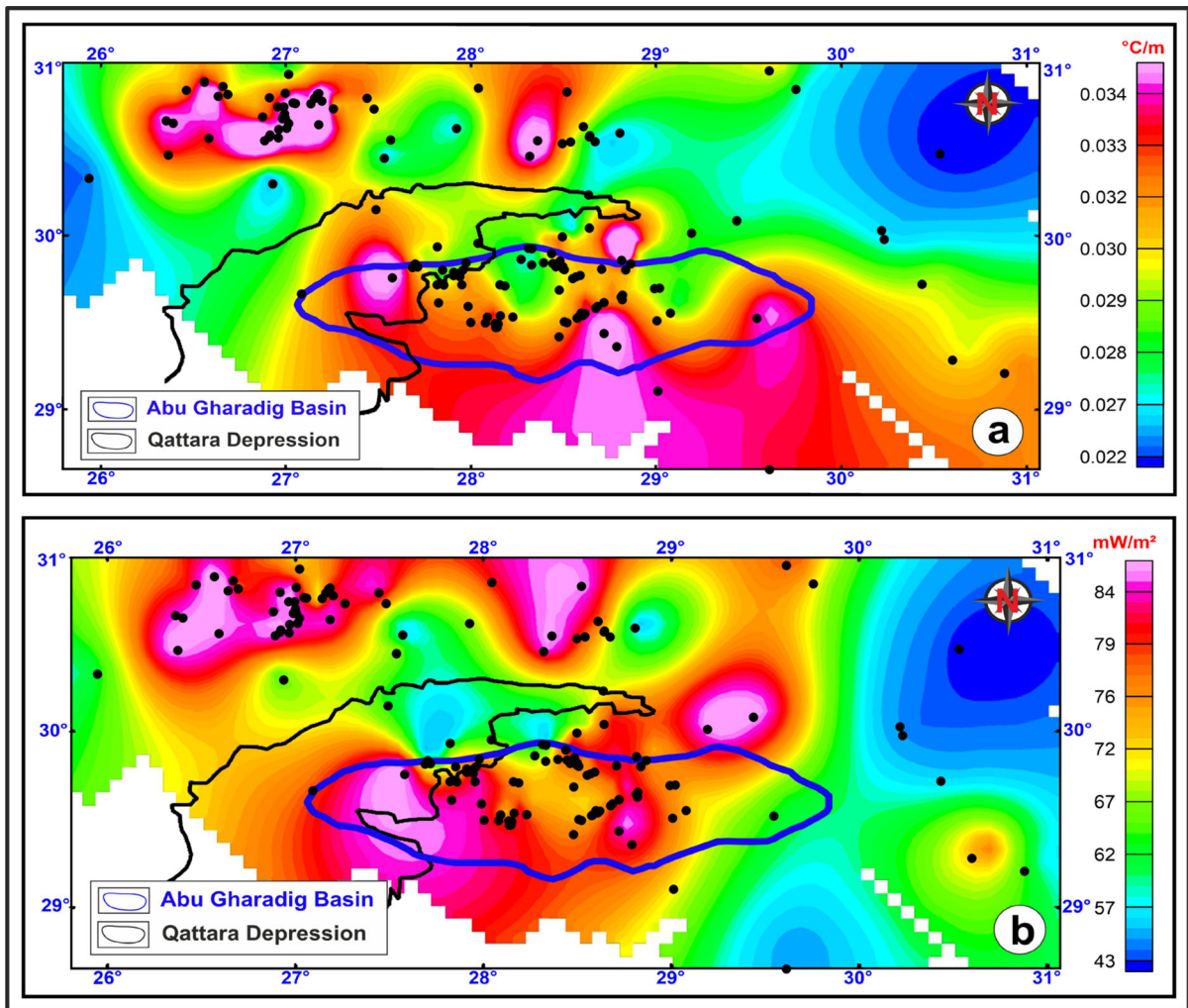


Figure 7

a Temperature gradients map and b heat flow map of AGB estimated from the corrected BHT data. Black dots indicate the locations of the used oil and gas wells where the bottom temperatures were recorded

$$TG = (T - T_s) / Z = dT / dZ \quad (3)$$

In which TG refers to the temperature gradient (geothermal gradient) in degrees Celsius per metre, T refers to the formation temperature, T_s refers to the yearly temperature at the surface and supposed to be 26.7 degrees Celsius according to Morgan et al. (1983), Z refers to the overall depths. We may also compute the heat flow Q from the temperature gradient by utilizing the formula (Tanaka et al., 1999; Turcotte and Schubert, 1982):

$$Q = \lambda(dT / dZ) \quad (4)$$

In which Q refers to the heat transfer and λ refers to the thermal conductivity coefficient, which suggest values of the stratigraphic Section (1.8–2.6 W/m °C) in the NW Desert that estimated by (Morgan et al., 1983).

4.2. CPD, Heat Flow and Temperature Gradient Estimates from TMI Data

Prior to utilizing TMI data for calculating the CPD, a reducing to pole (RTP) filter was applied with

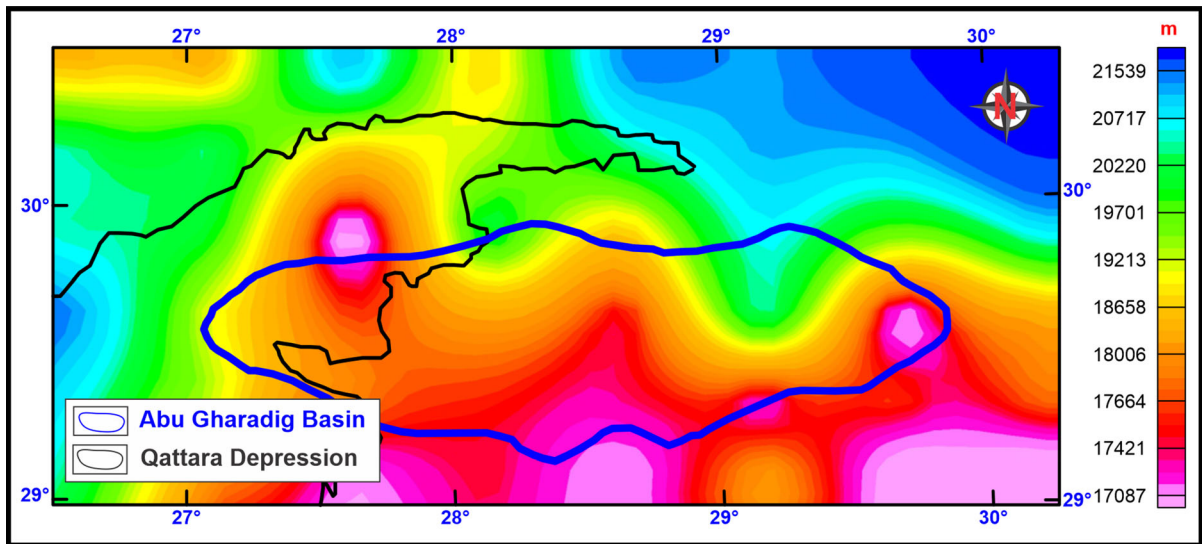


Figure 8
CPD map of the study region produced from power spectrum computations of aeromagnetic data

the magnetic declination of 4.426° and the magnetic inclination of 43.335° to reduce inclination-induced anomaly asymmetry and detect anomalies above the causative bodies (Fig. 3b). The CPD is the crustal depth at which magnetic minerals undergo a phase transition from ferromagnetic to paramagnetic due to an increase in temperature. The technique of centroid was used to integrate aeromagnetic data with spectrum analysis, where the CPD is assumed to indicate the base depth of the source of magnetic (Bhattacharyya & Leu, 1975; Okubo et al., 1985). Blakely (1995) goes into great detail regarding the theory of power spectrum analysis. The results from BHT data were used for verifying the outputs of CPD. Figure 4 summarized the methodology used for CPD estimation.

The magnetic layer in the horizontal direction becomes extremely broad and therefore the horizontal scale of the source of magnetic is larger than the distance from the top to the magnetic sources (Tanaka et al., 1999). In such computations, the depth precision is restricted to the width of the aeromagnetic window (L), hence we utilized $(L/4\pi)$ to calculate the greatest depth of CPD (Shuey et al., 1977). Expanding the aeromagnetic map's area and using more data allowed for more accurate

calculations; the area was divided into 48 overlapping square sub-areas (windows) with diameters of $(87 \times 113 \text{ km})$, and the radial average of the power spectrum of each window was calculated. The black dots in (Fig. 3b) depict the locations of the windows centers. The distance from the top to the magnetic source's Z_t was computed utilizing the gradient of the greatest wavelength portion of the spectrum, which was drawn with the wavenumber K , and the spectrum is split by each block's "K" rate and sketched against the wavenumber K to estimate the distance to the centroid Z_0 . Data's power spectrum from the airborne magnetic anomaly in sub-area no. 48 is depicted in (Fig. 5). Then basal depth Z_b which represents CPD was computed according to (Tanaka et al., 1999):

$$Z_b = 2Z_0 - Z_t \quad (5)$$

Given the temperature at CPD (580 degrees Celsius), the temperature gradient dT/dZ through the surface of the Earth could be estimate by (Maden, 2010; Stampolidis et al., 2005):

$$dT/dZ = (580 \text{ degrees Celsius} / Z_b) \quad (6)$$

The heat fluxes were computed by multiplying the temperature gradients by the heat conductivity, assuming there was no radioactive source, supposed

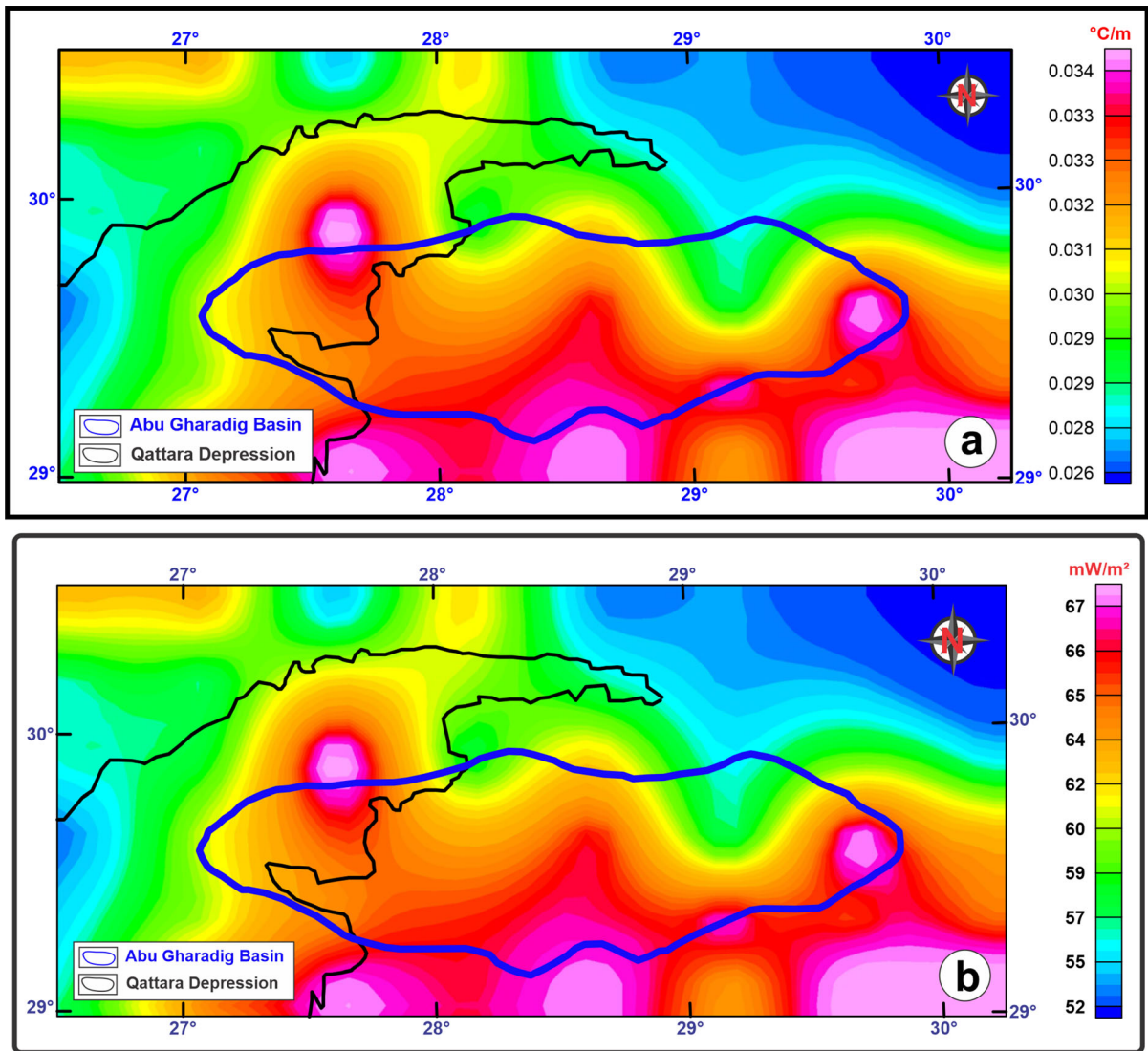


Figure 9

a Temperature gradients map of AGB based on aeromagnetic data-derived Curie depths and **b** heat flow map of AGB using thermal conductivity of $2.0 \text{ W/m } ^\circ\text{C}$ for the Precambrian basal crust

to be 2.0 W/mK representative of bottom crust of the Precambrian (Seipold, 1992).

4.3. 3D Inversion of Gravity Data

The main aim of 3D gravity inversion is to create a model of density that matches the gravity data and displays underlying density anomalies and geological features. Using GRABLOX-1.6 software (Pirttijärvi, 2004), our model considers a two-layer situation in

which a sedimentary layer lies above a basement layer. Figure 6 depicts the initial model, which is a rectangular superblock separated into parts of smaller size with parameters relating to the densities and thicknesses of underlying geologic strata. Each minor block is given its own fixed density parameter. Since we mainly used two layers, the height of each individual block is optimized only via the inversion approach to reduce the discrepancy between the observed and calculated gravity data. Utilizing a

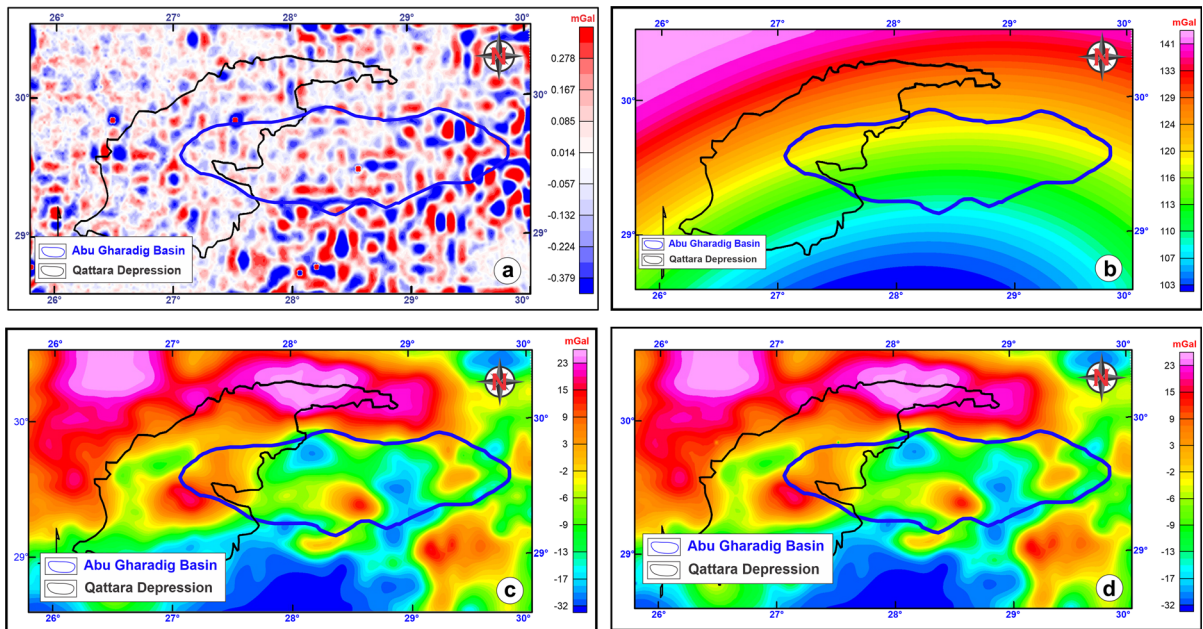


Figure 10

The 3-D density inversion results include **a** errors resulting from the disparity between measured and estimated gravity data, **b** Regional gravity filed, **c** Observed gravity data, and **d** modelled gravity data

constant density contrast, height inversion permits analysis of the thickness fluctuations of the sedimentary cover. The optimization approach employs Occam's principle, whereby both model roughness and data misfit are minimized. Optimization was also performed on the parameters of a 2nd-order polynomial defining a base anomaly.

The model stretches 50 km north to south (using 50 grid blocks) and 80 km east to west (using 80 grid blocks). The buffering effect was achieved by adding three extra blocks to the model as margins that have no influence on the computational area. Thus, the block model has (9632) small blocks as well as the model's novel discretization (XYZ) is ($86 \times 56 \times 2$ blocks) with a block size of ($3595.7 \times 4785.9 \times 4000$) m as the default. The block dimension remains unchanged throughout the block's depth. Based on the average densities of the major lithological units in the AGB, as well as a comparison of various densities of rocks recorded in the literature, the average densities for sedimentary and basement rocks were estimated to be 2.2 g/cm^3 and 2.67 g/cm^3 , respectively (Kearey & Brooks,

2002). These densities were obtained from logs of Formation Density Compensated (FDC) from certain hydrocarbon wells in Egypt's NW Desert (Abu El Ata, 1985).

5. Results

Based on the corrected BHT data from the oil and gas wells, the geothermal gradients and heat flow maps of AGB are shown in Fig. 7. Geothermal gradients vary from $0.022 \text{ }^\circ\text{C/m}$ to $0.034 \text{ }^\circ\text{C/m}$, with an average of $0.03 \text{ }^\circ\text{C/m}$, whereas the heat flow varies between 43 and 84 mW/m^2 , with an average of 72 mW/m^2 . Significant increases in heat flow values can be observed in the study area's central section, as well as in the eastern and northwest trends.

On the other hand, aerial magnetic data was used to determine Curie surface in order to estimate the thermal structure of the Earth's crust in the AGB. The original RTP map of the AGB has values range from -163 nT to 177 nT (Fig. 3b) and shows number of positive and negative anomalies that may be created

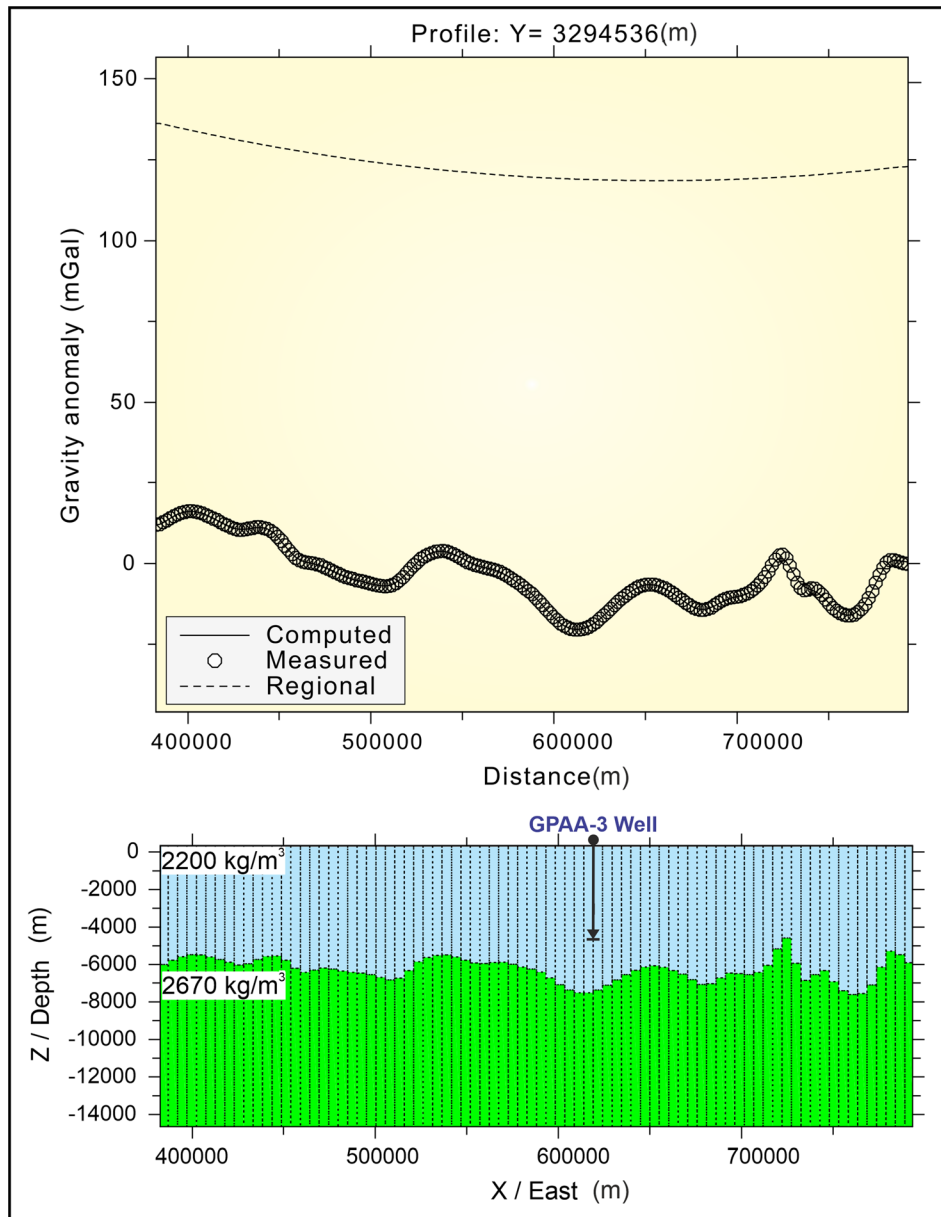


Figure 11

Example of E-W slice from a 3-D block traversing the GPAA-3 well. The density model arises from matching the observed (circles) and computed (lines) curves. Projected coordinates (UTM zone 35N) are given in meters

by the uplift and subsidence of foundation rock and its related structures, since sedimentary layers are often nonmagnetic or weakly magnetic and the magnetic layer is constrained above the Curie depth. Positive magnetic anomalies can be seen in the NE, NW, and Central parts of the map, indicating

shallower subsurface magnetic sources, but deeper magnetic sources can be found in other areas of the map. The map of CPDs for the AGB was mapped using a minimal curvature interpolation for Z_b , with a range of 17 to 21 km and an average of 19 km (Fig. 8). It reveals the existence of two grabens with

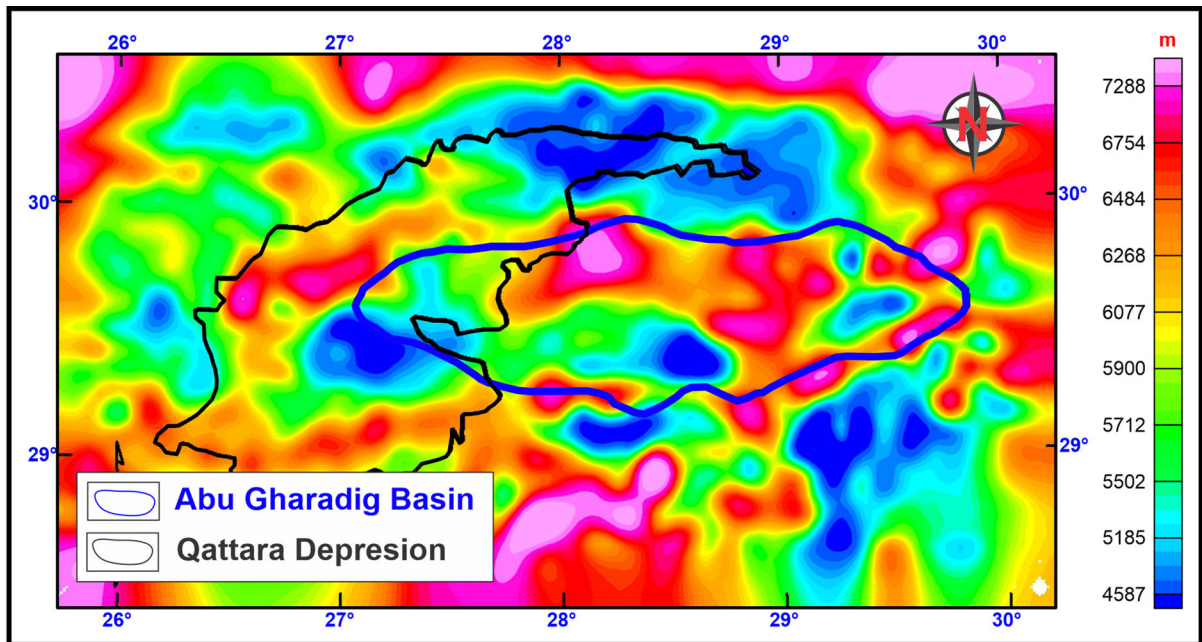


Figure 12
A relief map of the basement rock of AGB obtained from the outcomes of 3-D gravity data inversion

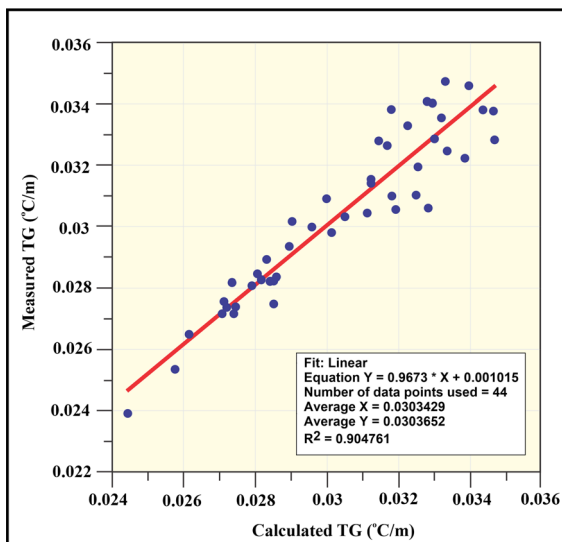


Figure 13
Correlation between measured temperature gradients from BHT (real data) and those derived from CPD (predicted data)

increasing depths in the eastern and northwestern parts and extending to the central region of the research area.

With the use of the CPD values, temperature gradients and heat flow maps of the AGB were produced (Fig. 9). The values of geothermal gradients are between 0.026 and 0.034 °C/m and an average of nearby 0.03 °C/m. The higher geothermal gradients are generally related to the shallow CPD areas, while the calculated heat flux rates range from 52 to 67 mW/m² and an average of nearby 60 mW/m² and that deemed exemplary of continental crust (Brott et al., 1976). The heat flux increases in the Eastern, NW trend and the central regions of the research area.

The Bouguer anomaly map in the AGB (Fig. 3a) exhibits values ranging from -32 mGal to 20 mGal, with positive values indicating that the sedimentary layer thickness is decreasing and vice versa. The gravity model is a crucial stage in gravity interpretation since it helps us grasp and know the depth, density, and structure of objects beneath the surface. The findings of the 3D model of gravity data are shown in Fig. 10 including the observed, modeled, regional (base) and error maps. The initial Bouguer gravity map and the crustal model gravity map have a lot in common. The error, defined as the difference between measured and computed gravity readings

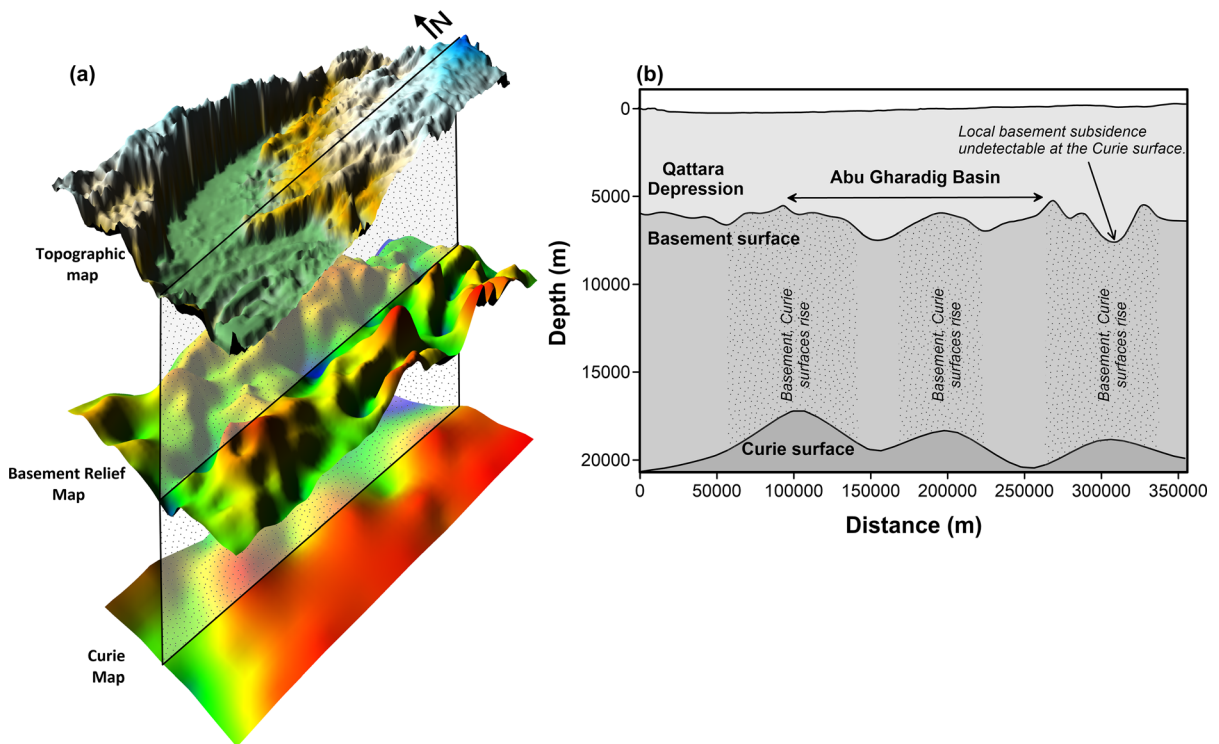


Figure 14

a Comparative 3D representations of the topographic, basement relief, and Curie depth maps of the study area, and **b** collected E-W profile that extracted from the exhibited maps and crossed the AGB

and is situated very nearby zero mGal. The conducted model has a Root Mean Square (RMS) value of 0.007. Unfortunately, there are no wells reached to the basement, so we make a comparison to know the rate of agreement of the thickness of sedimentary rocks with the present wells. Figure 11 shows the optimized model of X-section crossing well GPAA-3.

The entire thickness of the sedimentary layer resulting from the 3D inversion of gravity data was interpolated and mapped (Fig. 12). The study area is characterized by thick sedimentary cover, with elevations ranging from 4500 to 7000 m and beyond. A high correlation exists between the depth of the expected basement depending on a 3D gravity inversion and well data. The basement rock depths in the northwest, eastern and central regions of the research region are shallow, ranging from 4 to 5 km.

6. Integration and Discussion

Airborne gravity and magnetic measurements, together with BHT, are extremely beneficial for studying the geothermal structure of the AGB. First, analyses of aeromagnetic data verified by BHT data were used to study the thermal characteristics of the AGB. Power spectral analyses of magnetic measurements were utilized to find out the distribution of CPD beneath the research area. Generally, the AGB shows a deeper CPD (17–19 km). CPDs are always proportionate to the geological environment, with deeper CPDs (20 km to 30 km) found in stable continental areas and plateaus, and surface CPDs (about 10 km) located in volcanoes and geothermal locations (Tanaka et al., 1999). The AGB is located on the unstable shelf zone that is distinguished by surface tectonic features such as lateral pressures induced by numerous compressional processes like the folds of

the Syrian Arc (Schlumberger, 1984). It does, however, have geothermal conditions comparable to those seen on stable continents.

The geothermal gradient from CPDs and those from BHT are highly correlated, with roughly 90% agreement (Fig. 13). An average temperature gradient of 30 °C/km and a heat flow of around 60 mW/m² indicate the existence of low-temperature hydrothermal resources, which are more common in regions with a longer geological history and/or greater stability. It is well known that there is a positive relationship between petroleum occurrence and temperature gradient and heat flow rates, implying that petroleum production and full maturation happens when geothermal resources are present. By superimposing the AGB sedimentary basin map over the heat flow map, it should be possible to pinpoint areas that have thermally mature sedimentary rocks with greater hydrocarbon production potential than others.

Furthermore, the gravity technique is employed to delineate the basement surface below AGB, depending on the varying densities of rocks. Generally, the AGB is characterized by very thick sedimentary cover (4500–7000 m).

The changes in the depths of the basement rock are compared to the variations in CPD in order to determine the dependability of the Curie surface's influence on the thermal structure of the study area. Thus, CPD and depth to basement rocks variations were gathered and painted along a longitudinal profile passing across the AGB using 3D gravity inversions (Fig. 14). Shallow CPD and uplifts in the Precambrian basement rocks were found to have a link, indicating that the Precambrian basement rocks are responsible for significant heat flow locations in the AGB. Thus, the sedimentary cover is might be free of any radioactive sources that might contribute to the formation of additional heat inside the sedimentary section.

7. Conclusions

Geophysical data (airborne gravity and magnetic) and well logs data were investigated using the geothermal resources in the AGB, Northern Western Desert, Egypt. Corrected BHT data was used to

calculate the temperature gradient map (revealed values range 0.022–0.034 °C/m) and heat flow map (revealed values range 43–84 mW/m²) of the research region. The power spectral approach was used to determine CPD depths in the research region using aeromagnetic data (revealed values range 17–21 km). CPDs are more than 20 km in many regions, proportionate with results from stable continental areas and plateaus. The shallower CPDs of > 19 km in depth, that are present in the Eastern trend and NW trend also in the central part of the AGB, we can interpretation that where the crustal is thin and may appear the promising regions of geothermal exploration. From the curie point temperature of 580 degrees Celsius the geothermal gradients were computed and gives values from 0.026 to 0.034 °C/m, also from the geothermal gradients we can compute the heat flow that give values from 52 to 67 mW/m². The geothermal gradient from BHT and the geothermal gradient from CPDs are highly correlated, with a 90 percent agreement between the two data sets.

The depths to the basement surface were determined using a 3D gravity inversion, representing the sediment and basement interface according to a contrast density. The topography of the basement surface is intensively uneven and depth range from 4500 to 7000 m according to the results of 3D inversion. The calculated basement depth and that obtained from well data (well GPAA-3) were found to be extremely consistent. Combining the findings shows a consistency between shallow curie depths, uplifts on basement rocks, and locations of higher heat flow, suggesting that basement rocks are primarily responsible for geothermal potentiality on the AGB. Future research is proposed to include a more in-depth examination of regions with higher heat flows and the collection of ground water samples from the wells for geochemical investigations.

Acknowledgements

The authors are thankful to Dr. Valentin O. Mikhailov, editor of the Journal of Pure and Applied Geophysics, and the anonymous reviewers for the time and effort they devoted to increasing the quality

of the work via their comments and suggestions. The authors would like to express their gratitude to Eng. Haytham Gawish, Traffic Tunnels Director at Concord for Engineering and Contracting in Egypt, for his assistance in data collection, as well as Dr. Annette Goodfellow, head of a unit manager at Edinburgh Health Care in Scotland, for proofreading. Also, the authors are thankful to Dr. Markku Pirttijärvi, chief geophysicist at Radai Ltd. company in Finland, for using the Grablox software that he developed.

Funding

Open access funding provided by The Science, Technology & Innovation Funding Authority (STDF) in cooperation with The Egyptian Knowledge Bank (EKB).

Data Availability

The data that support the findings of this study are available from the corresponding author upon reasonable request.

Declarations

Conflict of interest The authors declare no conflict of interest.

Open Access This article is licensed under a Creative Commons Attribution 4.0 International License, which permits use, sharing, adaptation, distribution and reproduction in any medium or format, as long as you give appropriate credit to the original author(s) and the source, provide a link to the Creative Commons licence, and indicate if changes were made. The images or other third party material in this article are included in the article's Creative Commons licence, unless indicated otherwise in a credit line to the material. If material is not included in the article's Creative Commons licence and your intended use is not permitted by statutory regulation or exceeds the permitted use, you will need to obtain permission directly from the copyright holder. To view a copy of this licence, visit <http://creativecommons.org/licenses/by/4.0/>.

Publisher's Note Springer Nature remains neutral with regard to jurisdictional claims in published maps and institutional affiliations.

REFERENCES

- Abd El Aal, A., & Moustafa, A. (1988). Structural framework of the Abu Gharadig Basin, Western Desert, Egypt. In Proceedings of the 9th Egyptian General Petroleum Corporation Exploration and Production Conference, Cairo, pp. 23–50
- Abdel Zaher, M., Elbarbary, S., Sultan, S. A., El-Qady, G., Ismael, A., & Takla, E. M. (2018b). Crustal thermal structure of the Farafra Oasis, Egypt, based on airborne potential field data. *Geothermics*, 75C, 220–234.
- Abdel Zaher, M., Saadi, N. M., & Watanabeb, K. (2014). Geological applications potential of DEM, ETM+, and gravity data in arid and semi-arid regions with special reference to south Western Desert, Egypt. *Arabian Journal of Geosciences*, 7(5), 1705–1716.
- Abdel Zaher, M., Saibi, H., Mansour, K., Khalil, A., & Soliman, M. (2018a). Geothermal exploration using airborne gravity and magnetic data at Siwa Oasis, Western Desert, Egypt. *Renewable and Sustainable Energy Reviews*, 82, 3824–3832.
- Abdelzaher, M., Nishijima, J., Saibi, H., El-Qady, G., Masoud, U., Soliman, M., Youns, A., & Ehara, S. (2012). A Coastal aquifer study using magnetotelluric and gravity methods in Abo Zenema, Egypt. *Journal of Pure and Applied Geophysics*, 169(9), 1679–1692.
- Abu El Ata, A. (1985). Mapping the structural elements dissecting the Cretaceous rock units of the Qattara Depressions area, Western Desert, Egypt; using three-dimensional gravity modeling. Geological Survey of Egypt, Proc. of 4th Ann. M, pp. 103–123
- Atef, H., Abd El-Gawad, A., Abdel Zaher, M., & Farag, K. (2016). The contribution of gravity method in geothermal exploration of Southern part of the Gulf of Suez-Sinai region, Egypt. *NRIAG Journal of Astronomy and Geophysics*, 5, 173–185.
- Awad, G. (1984). Habitat of oil in Abu Gharadig and Faiyum Basins, Western Desert, Egypt. *AAPG Bulletin*, 68, 564–573.
- Ayyad, M., & Darwish, M. (1996). Syrian Arc structures, a unifying model of inverted basins and hydrocarbon occurrences in North Egypt. In Proceedings of the 13th Egyptian General Petroleum Corporation Exploration and Production Conference, Cairo, Vol. 1, pp. 40–59
- Bayoumi, A., & Lotfy, H. (1989). Modes of structural evolution of Abu Gharadig Basin, Western Desert of Egypt as deduced from seismic data. *Journal of African Earth Sciences*, 9, 273–287.
- Bhattacharyya, B., & Leu, L. (1975). Spectral analysis of gravity and magnetic anomalies due to two-dimensional structures. *Geophysics*, 40, 993–1013.
- Blakely, R. (1995). *Potential theory in gravity and magnetic applications*. Cambridge University Press.
- Boulos, F. (1990). Some aspects of the geophysical regime of Egypt in relation to heat flow, groundwater and micro-earthquakes. In R. Said (Ed.), *The geology of Egypt* (pp. 61–89). Balkema.
- Brott, C.A., Blackwell, D.D. & Mitchell, J.C. (1976). Geothermal Investigation in Idaho, Part 8, Heat Flow in the Snake River Plain Region, Idaho. 30. Department of Water Resources, Water Information Bulletin (195p)
- Chandrasekharan, D., Lashin, A., Al Arifi, N., Al Bassam, A., Varun, C., & Singh, H. (2016). Geothermal energy potential of Eastern Desert region, Egypt. *Environmental Earth Sciences*, 75, 697.

- Demerdash, N., Nehl, T., Fouad, F., & Arkadan, A. (1984). Analysis of the magnetic field in rotating armature electronically commutated dc machines by finite elements. *IEEE Transactions on Power Apparatus and Systems*, 7, 1829–1836.
- Dolson, J., Shann, M., Hammouda, H., Rashed, R., & Matbouly, S. (1999). The petroleum potential of Egypt. *AAPG Bulletin*, 83, 12.
- EGPC. (1992). In Western Desert, oil and gas fields, a comprehensive overview. Paper presented at the 11th Petroleum Exploration and Production Conference, Egyptian General Petroleum Corporation, Cairo, pp. 1–431
- El Ayouty, M. (1990). Petroleum geology. In R. Said (Ed.), *The geology of Egypt* (pp. 567–599). Rotterdam: A.A. Balkema.
- Elbarbary, S., Abdel Zaher, M., Mesbah, H., El Shahat, A., & Embaby, A. (2018). Curie point depth, heat flow and geothermal gradient maps of Egypt deduced from aeromagnetic data. *Renewable and Sustainable Energy Reviews*, 91, 620–629.
- Elbarbary, S., Araffa, S. A. S., El-Shahat, A., Abdel Zaher, M., & Khedher, K. M. (2021). Delineation of water potentiality areas at Wadi El-Arish, Sinai, Egypt, using hydrological and geophysical techniques. *Journal of African Earth Sciences*, 174, 104056.
- Green, C.M., Barritt, S.D., Fairhead, J.D. & Misener, D.J. (1992). The African magnetic mapping project. Extended abstract. European Association of Geoscientists and Engineers (EAGE) 54th Meet Technical Exhibition, Paris
- GSE. (1981). Geological survey of Egypt. *Geologic Map of Egypt, Scale, 1, 2000000*.
- Hantar, G. (1990). North Western Desert. In R. Said (Ed.), *The geology of Egypt* (pp. 293–319). Rotterdam: A.A. Balkema.
- Kearey, P., & Brooks, M. (2002). *An introduction to geophysical exploration*. Blackwell Scientific Publications.
- Labib, M. (1985). Contributions to the geology of Upper Cretaceous with special emphasis on Turonian–Senonian sedimentation patterns and hydrocarbon potentialities in the Abu Gharadig area, North Western Desert, Egypt. Unpublished Dissertation thesis, Geology Department, Cairo University, Cairo, p. 189
- Lashin, A. (2015). Geothermal resources of Egypt, country update. In Proceedings World Geothermal Congress, Melbourne, Australia, p.13
- Madani, A. (2020). Mapping Geothermal Anomalies in Rift-Related Wadi Natash Volcanic Field, South Eastern Desert, Egypt Using Thermal Infrared and SAR Remote Sensing Techniques, 13th International Geological Conference, 03-05 March 2020, Jeddah, Saudi Arabia. (Abstract)
- Madani, A., & Said, M. (2022). Satellite land surface temperature for mapping the geothermal anomalies in Egypt: A new contribution to the distribution of the geothermal plays. Submitted to Geothermal Energy Journal.
- Maden, N. (2010). Curie-point depth from spectral analysis of magnetic data in Erciyes stratovolcano (Central TURKEY). *Pure and Applied Geophysics*, 167, 349–358.
- Meshref, W. M. (1990). Tectonic framework of Egypt. In R. Said (Ed.), *The geology of Egypt* (pp. 113–155). Rotterdam: A.A. Balkema.
- Meshref, W.M., Beleity, A.E.H., Hammouda, H. & Kamel, M. (1988). Tectonic evolution of Abu Gharadig Basin. In: AAPG Bull; United States, vol. 72, No. CONF-8809346
- Mohamed, H. S., & Abdel Zaher, M. (2020). Subsurface structural features of the basement complex and geothermal resources using aeromagnetic data in the Bahariya Oasis, Western Desert, Egypt. *Pure and Applied Geophysics*, 177, 2791–2802.
- Mohamed, H. S., Senosy, M. M., & Abdel Zaher, M. (2016). Interactive interpretation of airborne gravity, magnetic, and drill-hole data within the crustal framework of the northern Western Desert, Egypt. *Journal of Applied Geophysics*, 134, 291–302.
- Morgan, P., Boulos, F. K., & Swanberg, C. A. (1983). Regional geothermal exploration in Egypt. *Geophysical Prospecting*, 31, 361–376.
- Okubo, Y., Graf, R. J., Hansen, R. O., Ogawa, K., & Tsu, H. (1985). Curie point depths of the island of Kyushu and surrounding areas, Japan. *Geophysics*, 50, 481–494.
- Rabeh, T., Bedair, S., & Abdel Zaher, M. (2018). Structural control of hydrogeological aquifers in the Bahariya Oasis, Western Desert, Egypt. *Geosciences Journal*, 22, 145–154.
- Saada, S. A. (2016). Curie point depth and heat flow from spectral analysis of aeromagnetic data over the Northern part of Western Desert, Egypt. *Journal of Applied Geophysics*, 134, 100–111.
- Said, R. (1962). *The geology of Egypt* (p. 377). Elsevier.
- Salem, R. (1976). Evolution of eocene-miocene sedimentation patterns in parts of northern Egypt. *AAPG Bulletin*, 60, 34–64.
- Schlumberger. (1984). In Geology of Egypt. Paper presented at the Well Evaluation Conference, Schlumberger, Cairo, pp. 1–64
- Schlumberger. (1995). In Geology of Egypt. Paper presented at the Well Evaluation Conference, Schlumberger, Cairo, pp. 58–66
- Seipold, U. (1992). Depth dependence of thermal transport properties for typical crustal rocks. *Physics of the Earth and Planetary Interiors*, 69, 299–303.
- Senosy, M. M., Youssef, M. M., & Abdel Zaher, M. (2013). Sedimentary cover in the South Western Desert of Egypt as deduced from Bouguer gravity and drill-hole data. *Journal of African Earth Sciences*, 82, 1–14.
- Sestini, G. (1995) Egypt. In H. Kulke (Ed.), Regional petroleum geology of the world, part II: Africa, America, Australia and Antarctica, Vol. Beiträge zur regionalen Geologie der Erde, Gebrüder Bornträger Verlagsbuchhandlung, Stuttgart. Bandolier, 22, 66-87
- Shazly, T. F. (2012). Geothermal modeling for Bahariya formation of basel-1x well, northern western Desert, Egypt, by using well logs analysis. *Journal of Applied Sciences Research*, 8, 753–762.
- Shuey, R. T., Schellinger, D. K., Tripp, A. C., & Alley, L. B. (1977). Curie depth determination from aeromagnetic spectra. *Geophysical Journal International*, 50, 75–101.
- Stampolidis, A., Kane, I., Tsokas, G. N., & Tsourlos, P. (2005). Curie point depths of Albania inferred from ground total field magnetic data. *Surveys in Geophysics*, 26, 461–480.
- Sultan, N., & Halim, M.A. (1988). Tectonic framework of Northern Western Desert, Egypt and its effect on hydrocarbon accumulations. In Proceedings of the 9th Egyptian General Petroleum Corporation Exploration and Production Conference, Cairo, Vol. 2, pp. 1–22
- Taha, M. A. (1992). Mesozoic rift basins in Egypt: their Southern extension and impact on future exploration. In Proceedings of the 11th Egyptian General Petroleum Corporation Exploration and Production Conference, Cairo, Vol. 2, pp. 1–19
- Tanaka, A., Okubo, Y., & Matsubayashi, O. (1999). Curie point depth based on spectrum analysis of the magnetic anomaly data in East and Southeast Asia. *Tectonophysics*, 306, 461–470.
- Telford, W.M., Gelbart, L.P., Sheriff, R.E., & Keys, D.A. (1990). Applied geophysics. Second edition Cambridge University Press, p. 770
- Turcotte, D. L., & Schubert, G. (1982). *Geodynamics*. Cambridge University Press.

- Waples, D. W., Pacheco, J., & Vera, A. (2004). A method for correcting log-derived temperatures in deep wells, calibrated in the Gulf of Mexico. *Petroleum Geoscience*, *10*, 239–245.
- Waples, D. W., & Ramly, M. (2001). A statistical method for correcting log-derived temperatures. *Petroleum Geoscience*, *7*, 231–240.
- Wood, D. (1984). The tectonic setting and structural evolutions of Abu Gharadig Basin, Western Desert of Egypt. *EGPC*, *250*, 250–235.

(Received February 26, 2022, revised October 2, 2022, accepted October 31, 2022, Published online November 10, 2022)